Infrared Spectroscopy of Model Electrochemical Interfaces in Ultrahigh Vacuum: Ionic versus Interfacial Solvation by Acetone and Acetonitrile on Pt(111)

Ignacio Villegas and Michael J. Weaver*

Contribution from the Department of Chemistry, Purdue University, West Lafayette, Indiana 47907

Received July 14, 1995[⊗]

Abstract: Infrared reflection−absorption spectroscopic (IRAS) measurements are reported for acetone and acetonitrile dosed onto Pt(111) in ultrahigh vacuum (uhv) both in the presence and absence of adsorbed potassium atoms at 90 K with the objective of elucidating the nature of cation solvation and its influence on surface−solvent interactions at these model electrochemical interfaces. Corresponding variations in the metal−uhv work function (Φ) evaluated with a Kelvin probe yield additional insight into the interfacial electrostatic environment as a function of the alkali and solvent exposure. Acetone and acetonitrile are particularly suitable solvents with which to evaluate the involvement of the surface on interfacial ion solvation, since both interact specifically with Pt(111). In both cases, chemisorption gives rise to vibrational signatures which are clearly distinguishable from those of the "bulk-like" multilayers, associated in particular with carbonyl ($\nu_{C=O}$) and C≡N stretching ($\nu_{C\equiv N}$) vibrations. Acetone and acetonitrile interact with the Pt(111) in two distinct fashions: the former binds via the oxygen lone pair of the carbonyl group, while the latter interacts via the nitrile π orbitals. In addition, the $\nu_{C=O}$ and $\nu_{C\equiv N}$ bands are sensitive to the coordination environment upon interaction with the cation. The present spectral evidence indicates that both solvents, despite the disparate nature of their surface interactions, reorient extensively to solvate K^+ *in preference* to the Pt surface, even for low K^+ fractional coverages ($\theta_K \sim 0.02$). The initial cation solvation by acetone yields the complete disappearance of the $\nu_{C=O}$ band at 1642 cm^{-1}, associated with chemisorbed acetone, being replaced by a weaker feature at 1678 cm^{-1} indicative of predominant interactions with K^+ instead. In the acetonitrile case, an IRAS band at 2243−9 cm^{-1} indicates coordination to K^+ via the nitrogen lone pair. In addition, the significant (ca. 0.3 eV) Φ increases observed upon ion solvation support the presence of negative-outward $^{\delta+}C{=}O^{\delta-}$ and $^{\delta+}C{\equiv}N^{\delta-}$ dipole orientations. Evidence of a substantial modifying influence of the metal surface on solvent−ion interactions, however, is provided by significant downshifts in the $\nu_{C=O}$ and $\nu_{C\equiv N}$ vibrational frequencies with respect to those observed in acetone and acetonitrile solutions of alkali cations. The present results call into question the validity of conventional models of electrochemical interfaces which treat the metal surface−solvent and ion−solvent interactions as separate problems: a substantial synergy between these phenomena is clearly evident.

Introduction

There is a remarkable evolution currently occurring in our fundamental structural understanding of metal−solution (i.e. electrochemical) interfaces. This is being driven by a number of related developments, especially from the expanding range of in-situ techniques such as scanning probe microscopies and X-ray methods which provide atomic-/molecular-level insight into spatial structure.[1,2] In helping to establish the subject of *electrochemical surface science* as a coherent research discipline, such developments bring about much closer and multidimensional ties between electrochemistry and conventional (i.e. traditional) surface science in ultrahigh vacuum (uhv) environments. This situation therefore provides renewed impetus to *uhv-based* studies of issues which are of direct importance to fundamental electrochemistry, especially topics that cannot be fully explored by means of in-situ techniques.

One uhv-based tactic of exceptional value in this regard, pioneered by Sass and co-workers in Berlin during the 1980's,[3,4] consists of examining the properties of interfaces formed by sequential co-dosing of the various "double-layer" components present at electrochemical interfaces. This so-called "uhv electrochemical modeling" approach not only provides a multifaceted experimental link between the physicochemical properties of in-situ electrochemical and uhv-based systems, but also enables the influences of the additional chemical components (solvent, ions, etc.) inevitably present at the former interface to be explored in a uniquely incremental fashion.[4]

An issue of central fundamental significance which is particularly amenable to uhv electrochemical-modeling tactics concerns elucidating roles of the solvent in determining the electrostatic double-layer and other interfacial properties. Traditionally, electrochemists have treated metal surface−solvent and interfacial ion-solvent interactions as largely separate, albeit related, problems.[5] However, the burgeoning molecular-level treatments of interfacial solvation prompted by contemporary experimental[6] and computational[7] approaches encourage consideration of their likely coupled nature.

As one aspect of a research program utilizing uhv electrochemical-modeling tactics, we have recently been exploring the

[⊗] Abstract published in *Advance ACS Abstracts,* December 15, 1995.

(1) For example, see: Lipkowski, J.; Ross, P. N., Eds. *Structure of Electrified Interfaces*; VCH Publishers: New York, 1993.

(2) Weaver, M. J.; Gao, X. *Annu. Rev. Phys. Chem.* **1993**, *44*, 459.

(3) (a) Sass, J. K.; Bange, K. *ACS Symp. Ser.* **1988**, *378*, 54. (b) Sass, J. K.; Bange, K.; Döhl, R.; Piltz, E.; Unwin, R. *Ber. Bunsenges. Phys. Chem.* **1984**, *88*, 354.

(4) For an erudite recent review, see: Wagner, F. T. in ref 1, Chapter 9.

(5) Conway, B. E. *Ionic Hydration in Chemistry and Biophysics*; Elsevier: Amsterdam, 1981.

(6) For example: Toney, M. et al. *Nature* **1994**, *368*, 444.

(7) For recent reviews, see: Schmickler, W. in ref 1, Chapter 6. Heinzinger, K. in ref 1, Chapter 7.

0002-7863/96/1518-0458$12.00/0

roles of interfacial solvation in the vibrational and electrostatic properties of chemisorbed neutral and ionic species on Pt(111).[8−13] We utilize as primary tools infrared reflection−absorption spectroscopy (IRAS) along with work-function measurements. The former not only yields quantitative information on solvent and other intramolecular adsorbate vibrations but also provides a direct link to in-situ electrochemical systems, since IRAS is also applicable (albeit with some restrictions) in this environment.[14] The work-function data supply invaluable information on the surface-potential changes induced by adsorbate dosing, thereby furnishing surface-potential profiles and providing the necessary bridge between the uhv-based and electrochemical potential scales.[3,4]

We have recently examined in some detail by IRAS and work-function measurements the solvation of an alkali-metal cation, K^+, on Pt(111) by the strongly H-bonded solvents water and methanol.[10−12] The choice of potassium was prompted by the capability of depositing accurately known coverages, θ_K, by gas-phase exposure of K atoms, the θ_K values being quantified from the marked work-function decreases that arise from K surface ionization. Marked changes are seen in the infrared intramolecular solvent frequencies with increasing solvent exposure, which can be understood in terms of progressive cation solvation. The important modifying influence of the metal surface upon the ionic solvation becomes clearly evident upon comparison with vibrational data for analogous progressive solvation of gas-phase cations.[10−13]

We present here results for the progressive solvation of K^+ on Pt(111) by acetone and acetonitrile. These archetypical nonassociating, yet strongly dipolar, solvents are of particular interest in the present context for several reasons. While both molecules provide strongly solvating media for cations such as K^+, resulting from their similar dipolar properties, acetone and acetonitrile are known to chemisorb on Pt(111) not only specifically but also in a very different (and spectrally distinguishable) fashion. While acetone binds to Pt(111) via a lone pair of the carbonyl oxygen,[15] acetonitrile adsorbs with the dipolar nitrile group lying flat.[16] This prompts an intriguing question: to what extent is this different surface chemistry (and consequent solvent dipolar orientation) that occurs in the absence of interfacial charge altered, or even eliminated, in the presence of ions such as K^+? It turns out that this issue, of central significance to interfacial electrochemistry, can be addressed insightfully for the present systems by IRAS. The present opportunity arises not only in view of the sensitivity of the carbonyl and cyano chromophores to the coordination environment but also because the intensities of these and other solvent vibrations are dependent on the molecular surface orientation via the well-known IRAS selection rule. These findings, along with attendant work-function measurements, point to a new level of understanding into the synergetic nature of ion−solvent and surface−solvent interactions at simple electrochemical interfaces.

Experimental Section

Experimental procedures involved in our uhv-based studies have been detailed elsewhere.[8,10] The experiments were performed in a stainless-steel chamber maintained at a base pressure of 2×10^{-10} Torr by means of turbo-, ion-, and titanium sublimation pumps. The infrared spectra were obtained with a Mattson (ATI) RS-1000 Fourier transform instrument equipped with a globar light source and a narrow-band MCT detector. As is conventional, all spectra are reported in a differential format, using solvent- and CO-free surfaces as references. Work-function changes with respect to clean Pt(111) were measured with a Delta-Phi Elektronik (Jülich, Germany) Kelvin probe. These measurements are accurate to 10 meV. The surface cleanliness was maintained by periodic Ar^+ sputtering and subsequent annealing to 1200 K. Carbon impurities were removed before each set of experiments by heating the sample to 900 K in 3×10^{-7} Torr of oxygen. All spectral measurements reported here were made at 90 K.

The solvents—acetone (Aldrich) and acetonitrile (Mallinckrodt)—were dosed through a nozzle located directly in front of the sample during IRAS experiments, enabling stepwise solvent exposure while maintaining the background pressure virtually unchanged. The continuous solvent exposure during work-function measurements required instead an increase of the vapor pressure in the chamber to 1×10^{-8} Torr. Solvent exposures in both cases were calibrated using temperature-programmed desorption (TPD) (vide infra). Gaseous impurities in the liquid solvents were removed by repeated cycles of freezing, pumping, and thawing. Mass spectra confirmed the purity of the vapors. As detailed in ref 10, calibration of the potassium coverages, dosed from a thoroughly outgassed SAES getter source, relied primarily on results obtained by Pirug and Bonzel which indicate a linear decrease in the Pt(111) work function with increasing potassium coverages between 0 and 0.08 monolayer (ML).[17] In cases where the potassium was postdosed onto the solvent film, the coverage was estimated from observed downshifts in the stretching frequency of atop carbon monoxide (ν^t_{CO}) on a saturated adlayer coadsorbed with the potassium.[10] A linear dependence of ν^t_{CO} as a function of potassium coverage ($\theta_K \leq 0.08$ ML) has been reported[18] (but see footnote 32 in ref 10). Finally, carbon monoxide (Airco) was dosed by raising the pressure in the chamber to appropriate values between 1×10^{-9} and 5×10^{-8} Torr. The CO and K coverages are expressed in monolayers (ML), as usual normalized to the Pt(111) atomic density.

Results

Temperature-Programmed Desorption. As mentioned above, TPD experiments were performed in order to calibrate the relative solvent coverages as a function of exposure. Using the integrated intensity of the TPD features, a linear dependence of the solvent coverage (θ^*_S) upon the exposure was ascertained uniformly for acetone dosed onto clean, CO-saturated, and K^+-precovered Pt(111). This linearity was maintained from submonolayer up to large multilayer coverages. Acetonitrile coverages on clean and CO-saturated Pt(111) also increased essentially in proportion to exposure. Since both the absolute coverage of the chemisorbed layers and the sticking coefficients of the acetone and acetonitrile on Pt(111) remain strictly speaking unknown, the exposures quoted in ensuing sections were normalized with respect to those required for saturation of the respective chemisorbed layers on clean Pt(111), denoted as an "equivalent monolayer" (EL), whereby $\theta^*_S = 1$.

Specifically, two desorption features were clearly distinguishable in the TPD curves ($m/e = 43$) for increasing acetone exposures onto Pt(111) at 90 K as shown in Figure 1 (solid

(8) (a) Kizhakevariam, N.; Jiang, X.; Weaver, M. J. *J. Chem. Phys.* **1994**, *100*, 6750. (b) Kizhakevariam, N.; Villegas, I.; Weaver, M. J. *Surf. Sci.* **1995**, *336*, 37.

(9) Kizhakevariam, N.; Villegas, I.; Weaver, M. J. *Langmuir* **1995**, *11*, 2777.

(10) Kizhakevariam, N.; Villegas, I.; Weaver, M. J. *J. Phys. Chem.* **1995**, *99*, 7677.

(11) (a) Villegas, I.; Kizhakevariam, N.; Weaver, M. J. *Surf. Sci.* **1995**, *335*, 300. (b) Villegas, I.; Weaver, M. J. *Electrochim. Acta*. In press.

(12) Villegas, I.; Weaver, M. J. *J. Chem. Phys.* **1995**, *103*, 2295.

(13) Villegas, I.; Weaver, M. J. *Surf. Sci.* Submitted for publication.

(14) Nichols, R. J. In *Adsorption of Molecules at Metal Electrodes*; Lipkowski, J., Ross, P. N., Eds., VCH Publishers: New York, 1992; Chapter 9.

(15) (a) Vannice, M. A.; Erley, W.; Ibach, H. *Surf. Sci.* **1991**, *254*, 1. (b) Sexton, B. A.; Hughes, A. E. *Surf. Sci.* **1984**, *140*, 227. (c) Avery, N. R. *Surf. Sci.* **1983**, *125*, 771. (d) Avery, N. R.; Weinberg, W. H.; Anton, A. B.; Toby, B. H. *Phys. Rev. Lett.* **1983**, *51*, 682. (e) Anton, A. B.; Avery, N. R.; Toby, B. H.; Weinberg, W. H. *J. Am. Chem. Soc.* **1986**, *108*, 684.

(16) (a) Ou, E. C.; Young, P. A.; Norton, P. R. *Surf. Sci.* **1992**, *277*, 123. (b) Sexton, B. A.; Avery, N. R. *Surf. Sci.* **1983**, *129*, 21.

(17) Pirug, G.; Bonzel, H. P. *Surf. Sci.* **1988**, *194*, 159.

(18) Tüshaus, M.; Gardner, P.; Bradshaw, A. M. *Surf. Sci.* **1993**, *286*, 212.

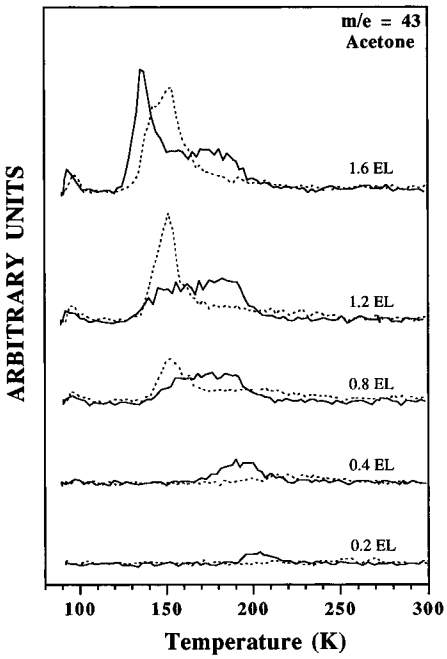

Figure 1. Temperature-programmed desorption (TPD) spectra at 3 K/s from 90 K for increasing acetone (m/e = 43) dosages as indicated obtained for either clean (solid traces) or K^+-proposed (θ_K = 0.020 ML, dashed traces) Pt(111).

traces). The higher-temperature feature due to desorption of chemisorbed acetone developed around 200 K at low exposures, progressively shifting to 180 K as the coverage was increased. The lower-temperature feature at 140 K, assigned to the desorption of multilayer acetone, appeared as the higher-temperature partner saturated. These results are consistent with literature reports.[15a−c]

In the presence of even low potassium coverages (down to $\theta_K \sim 0.02$), the "chemisorbed" acetone TPD feature is essentially removed, being replaced by a peak at ca. 150 K which becomes evident for coverages above 0.4 EL (Figure 1, dashed traces). This feature broadens toward lower temperatures as the solvent exposure increases. Noteworthy is the absence of a clearcut acetone TPD feature for low dosages, ≤0.4 EL, although a very broad weak feature could be discerned between 200 and 300 K.

Finally, some acetone decomposition occurs during the temperature-induced desorption as revealed by H_2 (m/e = 2) and CO (m/e = 28) TPD features observed at temperatures between 300 and 600 K. However, the integrated intensity of the CO desorption feature is virtually independent of the acetone dosage above 0.5 EL and corresponds to the decomposition of no more than 10% of the chemisorbed layer. A slightly smaller amount of CO was detected during desorption in the presence of K^+. However, no evidence of acetone decomposition to form adsorbed CO at 90 K was evident during our IRAS experiments (vide infra). Acetone decomposition has been associated previously with the formation of η^2-acetone on Ru(001), whereby the molecule binds with the carbonyl group parallel to the surface.[15d,e] This species has been detected on Pt(111) using electron energy loss spectroscopy (EELS) and IRAS only upon heating to temperatures near 200 K.[15a] Nevertheless, this complication is essentially negligible for the present purposes since the accuracy of the solvent exposures quoted here is no better than ±10%.

The TPD curves (m/e = 41) for increasing acetonitrile exposures onto Pt(111) at 90 K display a significantly more complex behavior. Two desorption features were observed at very low exposures, one at 350 K and the other at 220 K.

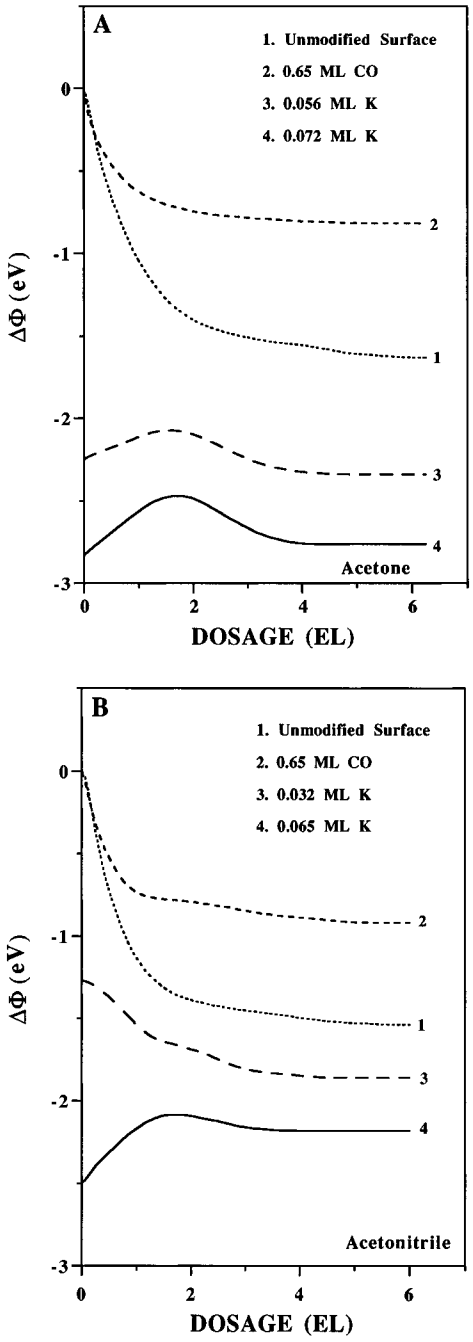

Figure 2. (A) Work-function changes (ΔΦ) induced by continuously increasing acetone exposures, expressed in equivalent monolayers (EL), onto Pt(111) with various K^+ and CO precoverages as indicated. (B) Work-function changes (ΔΦ) induced by continuously increasing acetonitrile exposures, expressed in equivalent monolayers (EL), onto Pt(111) with various K^+ and CO precoverages as indicated.

Increasing exposures led to a ca. 8 K downshift in the temperature of the latter and the eventual saturation of both. A third desorption feature emerged at 145 K upon saturation of the higher-temperature components. The higher-temperature features have been attributed to the desorption of chemisorbed acetonitrile, while the lower-temperature component corresponds to the desorption of condensed multilayers.[16] No acetonitrile decomposition was revealed by the TPD experiments.

Work-Function Changes. Work-function changes (ΔΦ) with respect to that of clean Pt(111) as a function of solvent exposure, θ_S^* (in EL units), are shown for acetone and acetonitrile in Figures 2A and 2B, respectively. The different ΔΦ-exposure curves in each figure correspond to solvent addition onto initially clean Pt(111) (curve 1) as well as onto Pt(111) modified by saturated CO adlayers (curve 2) and various

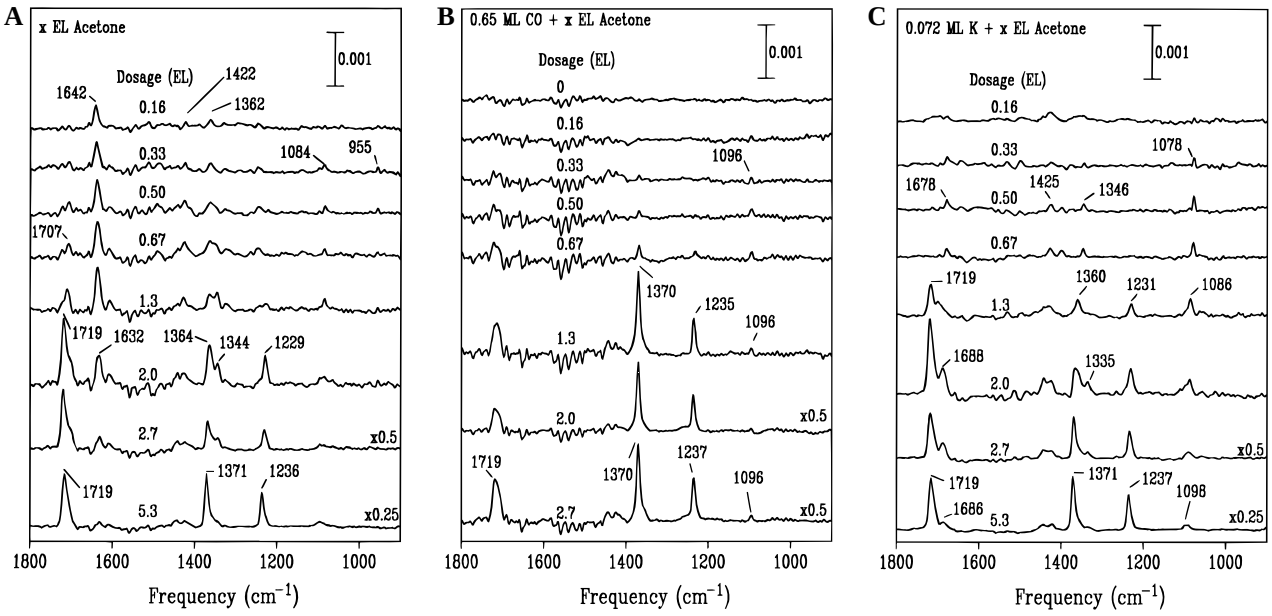

Figure 3. (A) Infrared spectra in the 900−1800-cm^{-1} region for increasing acetone exposures as indicated, in equivalent monolayers (EL), onto initially clean Pt(111). (B) Infrared spectra in the 900−1800-cm^{-1} region for increasing acetone exposures as indicated, in equivalent monolayers (EL), onto CO-saturated Pt(111) ($\theta_{CO} = 0.65$ ML). (C) Infrared spectra in the 900−1800-cm^{-1} region for increasing acetone exposures as indicated, in equivalent monolayers (EL), onto K$^+$-precovered Pt(111) ($\theta_K = 0.072$ ML).

potassium precoverages (curves 3 and 4). Multilayer acetone and acetonitrile exposures (≥4 EL) onto clean Pt(111) induced similar $\Delta\Phi$ decreases, ca. −1.6 and −1.5 eV, respectively. Furthermore, both solvents induce comparable $\Delta\Phi$ values corresponding to completion of the chemisorbed layer (1 EL). Smaller $\Delta\Phi$ values were obtained for multilayer acetone and acetonitrile dosed onto CO-saturated Pt(111), 0.8 and 0.9 eV, respectively (Figures 2A and 2B).

Such $\Delta\Phi - \theta_S^*$ data have been presented and discussed in an earlier report.[8b] Of particular interest here is the comparison of the $\Delta\Phi - \theta_S^*$ curves onto initially clean and K$^+$-predosed Pt(111). Representative examples of the latter are also shown for acetonitrile in Figures 2A and 2B, respectively (curves 3 and 4 in both cases). Note that the *y*-axis intercepts for each trace fall at substantially negative $\Delta\Phi$ values (ca 1.5−3 eV) for the θ_K values chosen, reflecting the well-known large Φ decreases attending K$^+$ adsorption. (Note that we refer here and below to adsorbed potassium formally as a *cation*, reflecting the likelihood of extensive surface ionization, especially in the presence of coadsorbed solvent.) Significantly, nonmonotonic $\Delta\Phi - \theta_S^*$ curves are obtained with both solvents for $\theta_K \geq 0.04$, the Φ values initially *increasing* (by up to ca 0.5 eV) before decreasing toward higher solvent exposures, $\theta_S^* \geq 1-2$ EL. The θ_K values, ≤0.07, employed here were selected primarily since they correspond to the range of surface concentrations typically encountered for nonspecifically adsorbed (i.e. diffuse-layer) cations at electrochemical interfaces. This suitability is also evident from the magnitude (≤1 eV) of the $\Delta\Phi$ decreases brought about by K$^+$ adsorption in the presence of excess solvent Figures 2A,B), corresponding to charge-induced decreases in the electrode potential of 1 V or less.

This $\Delta\Phi - \theta_S^*$ behavior is qualitatively similar to that reported recently for water and methanol dosing on K$^+$-precovered Pt(111), although larger initial Φ increases are observed with the latter solvents.[10,12] These $\Phi - \theta_S^*$ data provide insightful comparisons with corresponding IRAS responses upon progressive solvent exposure onto clean K$^+$-predosed Pt(111), which are now considered.

Infrared Spectroscopy. (a) Acetone. Infrared spectral sequences in the 900−1800-cm^{-1} region for increasing acetone exposures on initially clean, CO-saturated, and K$^+$-precovered Pt(111) are shown in Figures 3A, 3B, and 3C, respectively. The most diagnostic feature for submonolayer (<1 EL) acetone exposures on the clean surface is a band at 1642 cm^{-1} (cf. Figure 3A). As noted in earlier surface vibrational studies,[15] this feature can readily be assigned to the carbonyl stretching mode ($\nu_{C=O}$) of the acetone molecule bound to the metal via the oxygen lone pair in a η^1 configuration (vide infra). Weaker bands appear at 1422 and 1362 cm^{-1}, assigned to the asymmetric bending (δ^a_{Me}) and symmetric bending (δ^s_{Me}) modes of the methyl groups. Bands corresponding to the C−C−C asymmetric stretching (ν^a_{C-C-C}) and methyl rocking (ρ_{Me}) modes can also be detected at 1229 and 1084 cm^{-1}, respectively. For comparison, these frequencies along with those of the major bands in the 900−1800-cm^{-1} region for the bulk vapor, liquid, and solid acetone phases are listed in Table 1.[19,20] Also included are the band frequencies reported in an earlier IRAS study.[15a] Near completion of the first equivalent monolayer, a weak $\nu_{C=O}$ band emerges at 1707 cm^{-1}. Upon multilayer formation, bands grow in at 1719 ($\nu_{C=O}$), 1371 (δ^s_{Me}) and 1236 cm^{-1} (ν^a_{C-C-C}). Weaker bands are also observed at 1443 and 1424 (δ^a_{Me}) and 1096 cm^{-1} (ρ_{Me}) (Table 1).

Table 1. Comparison between the Infrared Frequencies of Bulk-Phase Vapor, Liquid, Crystalline, and Interfacial Acetone

			solid[b]		monolayer[d]		
mode	vapor[a]	liquid[a]	(Raman)	multilayer[c,d]	η^1	η^2	K$^+$
$\nu_{C=O}$	1731	1712	1697	**1719** (1716)	**1642** (1638)	(1610)	**1678**
δ^a_{Me}	1454	1445	1444	**1443** (1443)		(1445)	
	1435	1428	1431	**1424** (1422)	**1422** (1426)	(1426)	**1425**
			1426				
			1408				
δ^s_{Me}	1363.5	1360	1351	**1371** (1373)	**1362** (1350)	(1365)	**1346**
ν^a_{C-C-C}	1215.5	1220	1229	**1236** (1239)	**1246** (1238)	(1240)	
ρ_{Me}	1090	1090	1098	**1098** (1094)	**1084** (1086)	(1086)	**1078**

[a] From ref 19. [b] From ref 20. [c] For acetone exposure of 3−6 EL. [d] Data in parentheses taken from an earlier IRAS study by Ibach et al. (ref 15a).

(19) Dellepiane, G.; Overend, J. *Spectrochim. Acta* **1966**, *22*, 593.
(20) (a) Krause, P. F.; Glagola, B. G.; Katon, J. E. *J. Chem. Phys.* **1974**, *61*, 5331. (b) Harris, W.; Levin, I. W. *J. Mol. Spectrosc.* **1972**, *43*, 117.

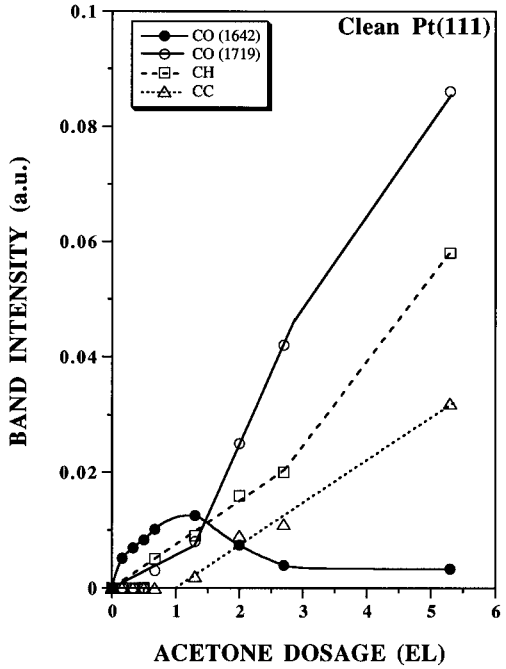

Figure 4. Integrated absorbance of various IRAS bands observed in the sequence of spectra shown in Figure 2A versus acetone exposure onto initially clean Pt(111): (●) carbonyl stretching ($\nu_{C=O}$) at 1636−42 cm^{-1}; (○) carbonyl stretching ($\nu_{C=O}$) at 1719 cm^{-1}; (□) methyl symmetric bending (δ^{s}_{Me}) at 1371 cm^{-1}; (△) asymmetric C−C−C stretching (ν^{a}_{C-C-C}) at 1236 cm^{-1}.

Interestingly, the chemisorbed carbonyl feature undergoes significant changes upon multilayer acetone exposure, downshifting about 10 cm^{-1} and becoming weaker (Figure 3A). Such infrared band intensity-exposure dependencies can be instructive in a more general vein. To this end, Figure 4 provides a plot of integrated intensity, *I*, of the chemisorbed (filled circles) and multilayer (open circles) carbonyl bands versus the acetone exposure. Also included for comparison are the corresponding $I - \theta^{*}_{S}$ traces for the ν^{a}_{C-C-C} and δ^{a}_{Me} vibrations (triangles and squares, respectively). Marked deviations from $I - \theta^{*}_{S}$ linearity (i.e. Beers' law) are seen in each case, which can provide insight into the structure of the solvent film (vide infra).

Progressive solvent exposure onto CO-saturated Pt(111) provides a worthwhile comparison with the spectral data since acetone chemisorption should thereby be altered drastically or eliminated. Acetone exposures below 0.67 EL onto CO-saturated Pt(111) yield no detectable infrared features other than a very weak ρ_{Me} band at 1096 cm^{-1} (Figure 3B). At higher exposures, however, additional multilayer-acetone bands appear at 1719 ($\nu_{C=O}$), 1370 (δ^{s}_{Me}), and 1237 cm^{-1} (ν^{a}_{C-C-C}).

Of primary interest here is the comparison with the spectral features for progressive solvent exposure onto Pt(111) predosed with K^{+}, where cation solvation should preferentially occur. Such a spectral set is shown in Figure 3C, on Pt(111) predosed with 0.072 ML of K^{+}. Comparison with spectra obtained on initially clean Pt(111) (Figure 3A) shows interesting differences, especially at low solvent exposures. Most strikingly, the chemisorbed carbonyl band seen at 1642 cm^{-1} on initially clean Pt(111) (Figure 3A) is now *entirely* absent, a weaker feature at 1678 cm^{-1} being evident instead at submonolayer acetone exposures (Figure 3C). The presence of predosed K^{+} also affects both the frequency and appearance of the other solvent vibrations under these conditions, the δ^{a}_{Me} and δ^{s}_{Me} bands being weakened and the ρ_{Me} mode being intensified in the presence of K^{+}. Qualitatively similar effects were observed for lower K^{+} coverages at least down to ca. 0.02 ML, the 1642-cm^{-1} chemisorbed $\nu_{C=O}$ band remaining absent. Typical multilayer

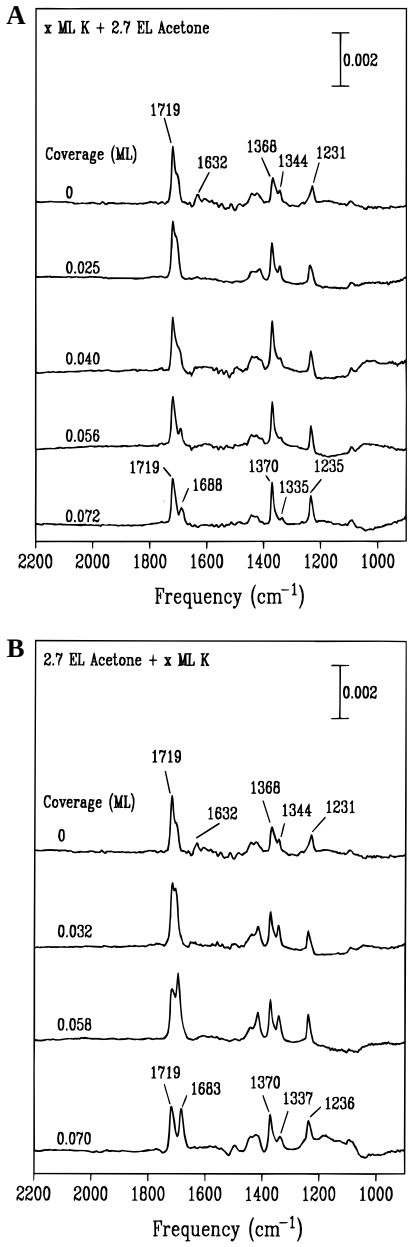

Figure 5. Infrared spectra in the 900−2200-cm^{-1} region for 2.7 EL of acetone on Pt(111) coadsorbed with increasing (A) predosed and (B) postdosed amounts of K^{+} as indicated.

spectral features appear as before above ca. 1 EL (Figure 3C). Nevertheless, a downshifted $\nu_{C=O}$ component at 1688 cm^{-1} is clearly present under these conditions, being related apparently to the "K^{+} solvation" $\nu_{C=O}$ feature at 1678 cm^{-1} seen at low acetone exposures (vide infra).

Further insight into the nature of the K^{+}−solvent interaction is provided by infrared spectra referring to increasing K^{+} coverages at a *fixed* acetone exposure. Figure 5A contains a representative set of such data for a sufficiently high acetone exposure, 2.7 EL, so that the interface should be fully solvated. Addition of even low K^{+} coverages, 0.025 ML, yields the complete elimination of the chemisorbed $\nu_{C=O}$ band (vide supra), the remaining C−C and C−H modes undergoing progressive changes that are complete by ca 0.05 ML of K^{+} (Figure 5A). Related experiments were also undertaken that entailed dosing the potassium *after* solvent exposure. Spectral results along these lines that refer to the same set of interfacial compositions as in Figure 5A are shown in Figure 5B. The latter, "postdosed-K^{+}" condition is seen to yield similar, yet more marked, K^{+}-induced spectral changes. In particular, the band at ca. 1685

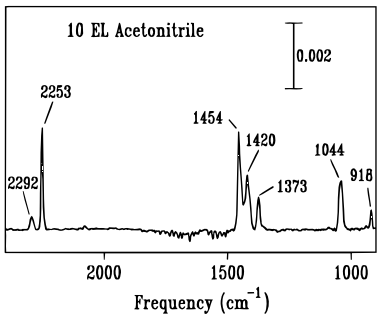

Figure 6. Infrared spectrum in the 900−2500-cm^{-1} region for ca. 10 EL of acetonitrile on clean Pt(111).

cm^{-1} attributable to "K^+ solvation" is significantly more pronounced in Figure 5B. These findings, consistent with more complete cation solvation under K^+ postdosing conditions, are reminiscent of the behavior seen with water and methanol dosing.[10,12]

(b) Acetonitrile. The major infrared spectral fingerprints for acetonitrile within the 900−2500-cm^{-1} region are evident in Figure 6, which is an IRAS spectrum corresponding to a large multilayer exposure, ca. 10 EL, on initially clean Pt(111). The band frequencies are also listed in Table 2, along with earlier IRAS data for the same system (given in parentheses)[16a] and the corresponding infrared bands for the bulk vapor, liquid, and crystalline phases.[21,22] As noted in Table 2, these bands are assigned to the C≡N stretching ($\nu_{C\equiv N}$), symmetric and asymmetric bending (δ^s_{Me}, δ^a_{Me}), methyl rocking (ρ_{Me}), C−C stretching (ν_{CC}), and ($\delta^a_{Me} + \nu_{CC}$) combination modes of the acetonitrile molecule.[21] Figures 7A, 7B, and 7C show spectral sequences in the $\nu_{C\equiv N}$ (2150−2350 cm^{-1}) region for increasing acetonitrile exposures onto initially clean, CO-saturated, and K^+-precovered Pt(111), respectively. The corresponding sequences in the $\rho_{Me} - \nu_{CC}$ (900−1200 cm^{-1}) region are shown in Figures 8A, 8B, and 8C. (We focus here only on these frequency segments rather than displaying the complete mid-infrared region in order to avoid possible confusion caused by interference from gas-phase water absorption from the spectrometer purge, worsened by the intrinsic weakness of some acetonitrile bands.) Acetonitrile exposures below ca. 1 EL onto clean Pt(111) yield no detectable bands in the $\nu_{C\equiv N}$ region, even though features attributed to the ρ_{Me} and ν_{CC} modes are clearly distinguishable at 1036 and 931 cm^{-1}, respectively (Figure 7A and 8A). These bands upshift to 1044 and 936 cm^{-1} with increasing acetonitrile exposure, displaying nonmonotonic changes in their intensity and bandwidth. Neither the symmetric nor asymmetric bending vibrational modes, however, were detectable for submonolayer acetonitrile exposures (cf. ref 16a). The band frequencies are listed in Table 2, along with the corresponding IRAS data reported for submonolayer exposures by Norton and co-workers[16a] and by Sexton and Avery using EELS.[16b] Note that the $\nu_{C\equiv N}$ band at 1615 cm^{-1} appearing in the submonolayer EELS spectra is not seen in IRAS, consistent with the proposed flat cyano group orientation.[16] Near the onset of multilayer growth, a $\nu_{C\equiv N}$ band emerges at 2253 cm^{-1}, close to the frequency for bulk-phase acetonitrile (Figure 7A). The $\nu_{C\equiv N}$ integrated band intensity plotted versus θ^*_S shows a linear response above a "threshold" exposure of ca 0.7 EL. The ($\delta^a_{Me} + \nu_{CC}$) combination band at 2292 cm^{-1} also becomes evident at large acetonitrile exposures (>2.7 EL). The onset of multilayer growth, however, is accompanied by marked *decreases* in the ρ_{Me} (1044 cm^{-1}) band intensity.

Submonolayer acetonitrile exposures onto CO-saturated Pt(111) result in a weak feature at 2321 cm^{-1} (Figure 8B), presumably due to a surface-induced upshift in the $\nu_{C\equiv N}$ mode (vide infra). The typical $\nu_{C\equiv N}$ band for multilayer acetonitrile (2253 cm^{-1}) again only emerges at exposures above ca. 0.7 EL. Nonetheless, ρ_{Me} (1042 cm^{-1}) and ν_{CC} (920 cm^{-1}) bands are clearly present in the spectra at submonolayer exposures (Figure 8B), even though they are broader and less intense, respectively, than for corresponding exposures on clean Pt(111) (Figure 8A).

In contrast to the spectral response on initially clean Pt(111), a $\nu_{C\equiv N}$ band at 2243 cm^{-1} is clearly distinguishable even for small fractional coverages of acetonitrile on K^+-predosed Pt(111) (Figure 7C). This feature upshifts to 2253 cm^{-1} as the first EL approaches completion. Further acetonitrile exposure yields growth of the multilayer peak at 2253 cm^{-1}. Also contrasting the response on the clean surface, the ρ_{Me} and ν_{CC} bnds at 1040 and 916 cm^{-1} are detected only at multilayer exposures on K^+-predosed Pt(111), displayig instead a series of very weak peaks in the 1000−1100-cm^{-1} region for exposures below 1 EL (Figure 8C). The band frequencies observed for monolayer acetonitrile in the presence of K^+ are also listed for comparison in Table 2.

As before, additional information concerning the K^+−acetonitrile interfacial interactions is provided by a series of spectra for a fixed amount of acetonitrile (2.7 EL) in the presence of increasing pre- and postdosed K^+ coverages, as shown in Figures 9A and 9B, respectively. Although there is no detectable change in the $\nu_{C\equiv N}$ band frequency with increasing K^+ precoverages, a significant increase in band intensity is evident (Figure 9A). In contrast, postdosing K^+ onto the acetonitrile-covered surface induces a marked broadening of the $\nu_{C\equiv N}$ band, which upshifts to 2259 cm^{-1} with increasing K^+ coverage while a shoulder develops at 2232 cm^{-1} (Figure 9B).

Discussion

Both solvent exposure-dependent infrared intensities and frequencies convey interesting implications concerning the influence of the ionic charge on the structure and orientation of the interfacial dipolar solvents. For convenience, we consider first the structural interpretation of the IRAS and work-function measurements for solvent on uncharged Pt(111), followed by the effects of K^+ exposure.

As already mentioned, the appearance of a markedly downshifted $\nu_{C=O}$ feature at 1642 cm^{-1} for submonolayer acetone exposures onto clean Pt(111) indicates the presence of end-on (η^1) bonding via the oxygen,[23] with the carbonyl group tilted as depicted in Figure 10A.[15] While the observed saturation of this band intensity for $\theta^*_S \sim 1$ EL is expected on this basis, its attenuation toward higher acetone exposures as the "multilayer" $\nu_{C=O}$ feature at 1719 cm^{-1} develops (Figure 4) suggests that the η^1 state is perturbed in the presence of additional solvent. Combined IRAS/EELS data for this system suggested a partial transition from η^1 to η^2 bonding under these conditions,[15a] the latter state involving a flat C═O orientation which is thereby infrared inactive. Alternatively or additionally, the presence of multilayer acetone as signaled by the 1719-cm^{-1} feature may well induce another, more weakly adsorbed, state that displaces the chemisorbed acetone. This is suggested by the appearance of the 1707-cm^{-1} band (Figure 3A).

The expected absence of acetone chemisorption in the presence of a saturated CO adlayer is confirmed by the complete absence of the 1642-cm^{-1} $\nu_{C=O}$ band (Figure 3B). Moreover, the notably stronger intensity of the δ^s_{Me} relative to the 1719-

(21) (a) Vankateswarlu, P. *J. Chem. Phys.* **1951**, *19*, 107. (b) Parker, F. W.; Nielsen, A. H.; Fletcher, W. H.; *J. Mol. Spectrosc.* **1957**, *1*, 107.
(22) Marzicchi, M. P.; Dobos, S. *Spectrochim. Acta* **1974**, *30A*, 1437.
(23) Driessen, W. L.; Groeneveld, W. L. *Revl. Trav. Chim. Pays. Bas* **1969**, *88*, 977.

Table 2. Comparison between the Infrared Frequencies of Bulk-Phase Vapor, Liquid, Crystalline, and Interfacial Acetonitrile

					submonolayer		
mode	vapor[a]	liquid[a]	solid[b]	multilayer (IRAS)[c,d]	(IRAS)[d]	(EELS)[e]	K^+
$\delta^a_{Me} + \nu_{CC}$	2305			2292			
$\nu_{C\equiv N}$	2268	2254	2251	2253 (2252)		1615	2243−9
			2250				
δ^a_{Me}	1454	1443	1453	1454 (1455)		1435	
			1451	1420 (1420)		1435	
			1448				
δ^s_{Me}	1389	1375	1378	1373 (1373)		1375	
			1372				
ρ_{Me}	1041	1047	1048	1044 (1040)	1036−40 (1038)	1060	1030−1040
			1040				
			1036				
ν_{CC}	920	917	918	918 (918)	930−5 (930) (988)	950	

[a] From ref 21. [b] Data for the crystalline solid obtained from ref 22. [c] For acetonitrile exposure of 3−10 EL. [d] Data in parentheses taken from an earlier IRAS study by Norton et al. (ref 16a). [e] From ref 16b.

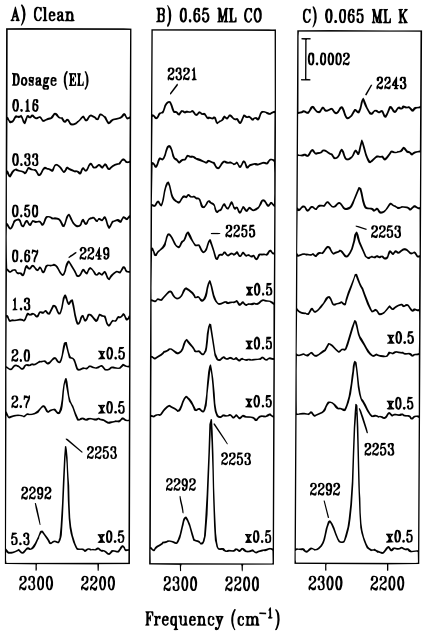

Figure 7. Infrared spectra in the $\nu_{C\equiv N}$ (2150−2350 cm^{-1}) region for increasing acetonitrile exposures as indicated, expressed in equivalent monolayers (EL), onto (A) initially clean, (B) CO-saturated (θ_{CO} = 0.65 ML), and (C) K^+-precovered (θ_K = 0.070 ML) Pt(111).

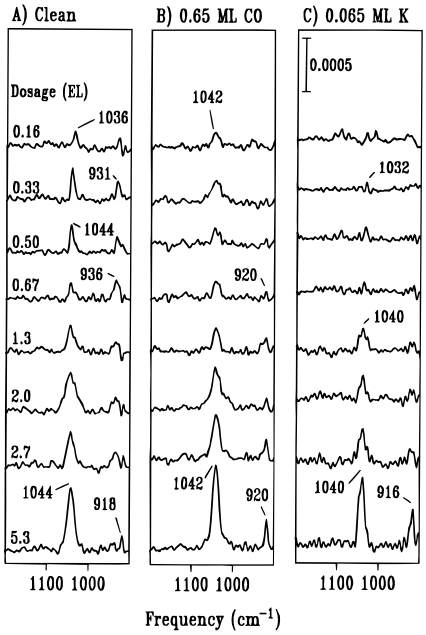

Figure 8. Infrared spectra in the $\rho_{Me} - \nu_{CC}$ (900−1200 cm^{-1}) region for increaisng acetonitrile exposures as indicated, expressed in equivalent monolayers (EL), onto (A) initially clean, (B) CO-saturated (θ_{CO} = 0.65 ML), and (C) K^+-precovered (θ_K = 0.070 ML) Pt(111).

cm^{-1} $\nu_{C=O}$ vibration seen for high ($\theta^*_S \approx$ 2 to 5 EL) acetone exposures on CO-modified compared with clean Pt(111) (compare Figures 3A and 3B) indicates that the surface template influences the adsorbate orientation, etc., even at the multilayer stage.

The present infrared data for submonolayer exposures of acetonitrile on Pt(111) are consistent with earlier EELS results[16b] which, as mentioned above, indicate the occurrence of binding with the cyano group parallel to the surface, as depicted in Figure 11A. The observation of a strongly downshifted EELS cyano feature at 1615 cm^{-1} (Table 2)[16b] provides more direct evidence along these lines given that the rehybridization associated with such Pt−cyano π bonding will leave an essentially double C−N bond.[16b] In addition to the expected lack of this cyano feature in the infrared spectra, Norton and coworkers noted the absence of the methyl bending vibrations along with an observed 30 cm^{-1} downshift of the methyl C−H stretches, and thereby suggested the occurrence of surface−acetonitrile interfactions involving the methyl as well as the cyano group.[16a] More straightforwardly, the appearance of the ν_{C-C} feature at 931−6 cm^{-1} for submonolayer acetonitrile exposures (Figure 8A) is entirely consistent with the adsorbate configuration depicted in Figure 11A. Thus the rehybridized nitrile carbon will necessarily form a C−C bond tilted from the surface plane, thereby making this vibration infrared active. The observed ca. 15 cm^{-1} upshift in the ν_{C-C} frequency for chemisorbed acetonitrile is also consistent with a diminution in the C−N bond order.

The presence of a saturated CO adlayer, as expected, also modifies markedly the exposure-dependent acetonitrile spectra. The virtual absence of the ν_{C-C} mode for submonolayer acetonitrile exposures (Figure 8B) suggests that the C−C, and possibly the C−N, bond is oriented flat on top of the CO adlayer. However, the appearance of the apparently upshifted $\nu_{C\equiv N}$ band at 2320 cm^{-1} (Figure 7) is suggestive of some end-on surface bonding via the nitrogen lone pair by analogy with analogous Pt(111)−acetonitrile complexes.[24] This conceivably occurs at surface sites created by lateral displacement of some adsorbed CO.

The spectra observed for both solvents in the presence of coadsorbed K^+ provide multifaceted insight into both the nature of progressive cation solvation and its attendant influence upon the surface−solvent interactions. We again consider first the

(24) Walton, R. A. *Spectrochim. Acta* **1965**, *21*, 1795.

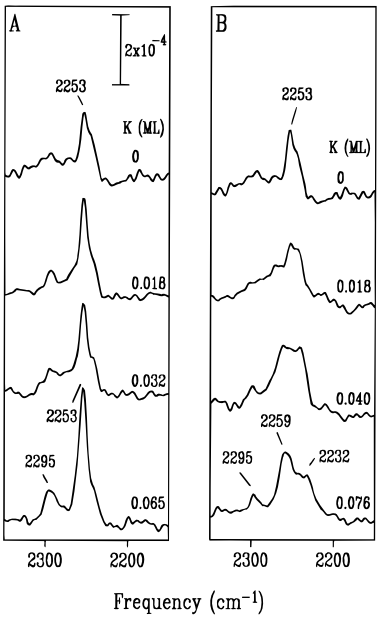

Figure 9. Infrared spectra in the $\nu_{C\equiv N}$ (2150−2350 cm^{-1}) region for 2.7 EL of acetonitrile on Pt(111) along with increasing (A) predosed and (B) postdosed amounts of K^+ as indicated.

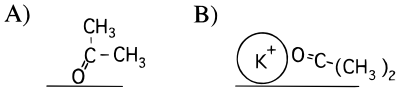

Figure 10. Schematics illustrating the acetone structures formed during the initial stages of (A) chemisorption and (B) interfacial K^+ solvation on Pt(111) (see text for details).

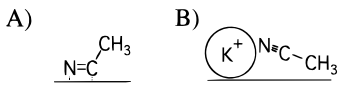

Figure 11. Schematics illustrating the acetonitrile structures formed during the initial stages of (A) chemisorption and (B) interfacial K^+ solvation on Pt(111) (see text for details).

data for acetone. The complete elimination of the chemisorbed carbonyl feature at 1642 cm^{-1} and its replacement by weaker bands at 1678−1688 cm^{-1} (Figures 3A and 3C) even at very low K^+ coverages attests to a profound *long-range* perturbation of the interfacial solvent configuration by the ionic charge. This striking deduction is also supported by the observed elimination of the "chemisorbed acetone" TPD feature even at similarly low K^+ coverages (Figure 1). The likely nature of the interactions involved is discussed further below.

The nature of the shorter-range ion−solvent interactions, i.e. the interfacial cation solvation, is clarified by several aspects of the IRAS results. Most directly, the $\nu_{C=O}$ band at 1678 cm^{-1} that develops for submonolayer acetone exposures is indicative of K^+ coordination via the carbonyl oxygen. Similar, albeit smaller, $\nu_{C=O}$ downshift from the uncoordinated $\nu_{C=O}$ frequency, 1720 cm^{-1}, have been observed for alkali cation solutions in acetone.[25] Some information on the likely cation-induced changes in solvent orientation can also be gleaned from exposure-dependent band intensities. The markedly (ca. 3−4 fold) smaller $\nu_{C=O}$ intensities of the 1678- versus 1642-cm^{-1} feature for submonolayer acetone exposures on clean Pt(111) (Figures 3A and 3C) suggest strongly that the carbonyl group is oriented more parallel to the metal surface, as depicted in Figure 10B. The attenuation of the δ^s_{Me} band intensity seen under these conditions (Figures 3A and 3C) can also be rationalized by changes in solvent orientation in the vicinity of the coadsorbed K^+.

The $\nu_{C=O}$ band at 1688 cm^{-1} that emerges for acetone exposures above ca. 1 EL (Figure 3C) may also be ascribed to acetone coordinated to, or at least associated closely with, the coadsorbed K^+. This notion is supported by the greater intensity of the ca. 1685-cm^{-1} feature upon postdosing, rather than predosing, K^+ with multilayer acetone films (Figure 5B versus Figure 5A) since the cation should thereby be more fully solvated. However, the high intensities of the 1685 cm^{-1} band—typically comparable to the 1719 cm^{-1} feature for uncoordinated acetone even for high acetone/K^+ stoichiometric ratios (≥10-fold)—suggest that this $\nu_{C=O}$ band may not arise entirely from acetone bound directly to the cation.

The corresponding infrared spectra for acetonitrile in the presence of K^+ (Figures 7 and 8) provide an intriguing comparison in that they indicate the occurrence of *similar* interfacial ionic solvation for these two solvents despite the marked dissimilarities in their surface coordination noted above. That a substantial K^+-induced reorientation of acetonitrile occurs is evident from the appearance of the $\nu_{C\equiv N}$ band at 2243−2253 cm^{-1} at submonolayer acetonitrile exposures in the presence of K^+, which is entirely absent on clean Pt(111) (Figures 7A and 7C). This finding demonstrates that at least a fraction of the adsorbed acetonitrile is transformed from the "flat" orientation (Figure 11A) to configurations such as that depicted in Figure 11B. The latter involves a tilted orientation and a recovery of the −C≡N triple bond, thereby having the linear C−C≡N configuration shown. While the nitrile vibrational feature by itself does not address the degree to which this solvent reorientation occurs, the behavior of the ν_{C-C} band is more revealing. Since, as noted above, the 931-6 cm^{-1} ν_{C-C} feature for chemisorbed acetonitrile (Figure 8A) signals the presence of the bent C−C═N configuration, the observed complete absence of this band in the presence of K^+ (Figure 8C) indicates that the cation-free observed configuration is *essentially removed*. This finding that the otherwise-dominant chemisorbed state of the solvent is drastically altered in the presence of low ionic coverages is intriguingly similar to the behavior of acetone noted above, despite the very different cation-free adsorbate configurations.

The significant (5−10 cm^{-1}) downshift of the $\nu_{C\equiv N}$ frequency seen for submonolayer acetonitrile on K^+-predosed Pt(111) (Figure 7C) also indicates the occurrence of direct K^+−solvent interactions. Alkali-metal cations dissolved in acetonitrile solvent yield instead slight (10−20 cm^{-1}) $\nu_{C\equiv N}$ upshifts.[26] This behavioral difference can be accommodated by postulating weak nitrile−surface π interactions, as can be anticipated from the solvent configuration as drawn in Figure 11B.

Further evidence supporting the occurrence of substantial cation-induced solvent reorientation is obtained by noting that the integrated intensity of the $\nu_{C\equiv N}$ band increases substantially, by 2- to 3-fold, for increasing K^+ coverages for both cation predosed and especially postdosed conditions (Figures 9A and 9B). Such intensity increases are expected from the infrared selection rule if the flat chemisorbed (i.e. infrared-inactive) nitrile group is tilted up by the K^+ coadsorption. As for the acetone case, the significant differences for predosed and postdosed K^+ (Figures 9A and 9B) are consistent with the

(25) (a) Lalić, M.; Jeremić, M.; Antić-Jovanović, A.; Bojović, V. *J. Mol. Liquids* **1988**, *39*, 105. (b) James, D.; Mayes, R. E. *Aust. J. Chem.* **1982**, *35*, 1775. (c) Perelygin, I. S.; Klimchuk, M. A. *Russ. J. Phys. Chem.* **1974**, *48*, 1466. (d) Wong, M. K.; McKinney, W. J.; Popov, A. I. *J. Phys. Chem.* **1971**, *75*, 56. (e) Minc, S.; Kecki, Z.; Gulik-Krzywicki, T. *Spectrochim. Acta* **1963**, *19*, 353. (f) Yamada, H. *Bull Chem. Soc. Jpn.* **1960**, *33*, 780. (g) Yamada, H. *Bull. Chem. Soc. Jpn.* **1960**, *33*, 667. (h) Pullin, A. D. E.; Pollock, J. McC. *Trans. Faraday Soc.* **1959**, *54*, 11.

(26) (a) Akopyan, S. Kh.; Denisova, A. S.; Solov'eva, L. *Russ. J. Phys. Chem.* **1989**, *63*, 999. (b) Perelygin, I. S.; Klimchuk, M. A. *Russ. J. Chem.* **1973**, *47*, 1138. (c) Coetzee, J. F.; Sharpe, W. R. *J. Soln. Chem.* **1972**, *1*, 77. (d) Kecki, Z.; Wojtczak, J. *Rocz. Chem.* **1970**, *44*, 847.

occurrence of complete cation solvation in the latter case. This is particularly evident from the small yet significant (6 cm^{-1}) *upshift* in the main $\nu_{C\equiv N}$ band frequency induced by K^+ postdosing (Figure 9B), which as noted above is compatible with "complete" K^+−acetonitrile solvation unmodified by solvent−surface interactions.

Of significant interest, particularly in an electrochemical context, is the nature of the interaction responsible for the removal of the chemisorbed solvent states by the presence even of low ($\theta_K \sim 0.02$) K^+ coverages. Qualitatively similar findings involving solvent coadsorption at metal−uhv interfaces have been reported earlier, primarily on the basis of TPD measurements.[4,27] For example, Kizhakevariam et al. noted that low Cl coverages on Ag(110) act to stabilize surprisingly large numbers of water molecules (up to 13 per Cl) as deduced by TPD.[28] In the present case, the K^+−solvent interactions clearly involve longer-range component(s) in that the essential removal of the chemisorbed solvent for $\theta_K \sim 0.02$ implies that this state is perturbed for solvent molecules as far as ca. 10 Å from a given K^+ species.

In the surface science literature, it is common to attribute such longer-range effects (i.e. those extending beyond the first 1-2 nearest neighbors) to indirect (or "through-metal") interactions.[4,29] To a certain extent, the former type may indeed be of importance here. Thus the removal of the η^1 acetone chemisorbed state by coadsorbed potassium may be induced by the increased metal electron density attending the alkali-metal ionization, discouraging the occurrence of oxygen−metal charge transfer. The opposite effect, involving the stabilization of the η^1 state by the coadsorption of electronegative species, has been observed for acetone−oxygen coadsorption on Ru(001), and explained similarly.[15d]

However, given that the present potassium−solvent coadsorbate system can usefully be considered to involve "ion-dipole" energetics, the likely longer-range nature of these electrostatic interactions should also be borne in mind. It is established that the solvation of univalent cations by dipolar fluids involves reorientation even within the third solvent shell, involving interactions of several kcal mol^{-1}.[30] A rough estimate of the stabilization of the acetone chemisorbed state by surface−carbonyl coordination can be gleaned from the ca. 40 K higher desorption temperature of this species versus the multilayer solvent (Figure 1). This temperature difference corresponds to an energy stabilization of ca. 2.5 kcal mol^{-1} by following the usual TPD analysis (cf. ref 28).[31,32] While our understanding of extended dipolar interactions within adsorbed layers remains decidedly incomplete,[33] there appear to be good reasons to anticipate important contributions from through-space as well as through-metal effects, especially for charged solvated interfaces.

It remains to consider the corresponding solvent-induced changes in the surface work function, $\Delta\Phi$, in the light of the IRAS data. The closely similar $\Delta\Phi - \theta_S^*$ responses for dosing acetone and acetonitrile monolayers onto clean Pt(111) (curve 1, Figures 2A and 2B) are perhaps surprising given that the spectral data indicate clearly that the dipolar carbonyl and nitrile groups involved attain markedly different orientations under these conditions. The conventional electrochemical picture of such work-function, and surface-potential ($\Delta\phi$), changes emphasizes the role of solvent dipole orientation: given the comparable gas-phase dipole moments of acetone and acetonitrile (2.9 and 3.9 D, respectively[34]), one would anticipate markedly larger $\Delta\Phi - \theta_S^*$ responses for the former solvent on this basis.[8b] However, as discussed in detail in ref 8b, this and other lines of evidence show that the marked (ca. 1−3 eV) Φ decreases commonly induced upon solvent exposure on clean metals such as Pt(111) are influenced importantly by other factors, particularly alterations in the surface electron distribution induced by molecular adsorption.[35]

Nevertheless, the nonmonotonic $\Delta\Phi - \theta_S^*$ responses observed for both acetone and acetonitrile exposure onto K^+-precovered Pt(111) (curve 4, Figures 2A and 2B) are entirely consistent with the models prsented above for interfacial cation solvation. Thus the initial Φ increases observed for $\theta_S^* \leq 1$ EL in both cases can be understood simply in terms of a dipolar solvent orientation with the negative pole tilted upward, induced by interaction with nearby cation−electron image ($K^+\cdots e^-$) dipoles. Additionally, and perhaps equivalently, one can envisage the Φ increases as involving partial screening of the $K^+\cdots e^-$ image dipoles, responsible for the substantial Φ decreases induced by such alkali-metal adsorption on clean Pt(111). The Φ decreases observed for multilayer solvent dosing onto K^+-precovered Pt(111), for $\theta_S^* \sim 2$ to 4 EL (Figures 2A and 2B), probably correspond to adsorption at surface sites removed from the cationic charges. However, the above IRAS data indicate clearly that the ionic charge influences the solvent configuration even under these conditions.

Concluding Remarks

The foregoing infrared spectral data provide a picture of dipolar solvation at charged metal interfaces that differs markedly from conventional wisdom in that even small cation coverages ($\theta_K \sim 0.02$) induce drastic alterations in the nature of the surface−solvent interactions. This finding applies to both dipolar solvents examined here, featuring "end-on" (acetone) and "side-on" (acetonitrile) surface binding of the dipolar moiety in the absence of ionic charge. The essential removal of these disparate chemisorption states and their at least partial replacement by solvent configurations reflecting electrostatic cation−dipole and the longer-range interactions calls into question the relevance of *charge-free* interfacial solvent models to *charged* electrochemical interfaces.

More generally, the present results are considered to provide a further testament to the virtues of infrared spectroscopy combined with uhv-based electrochemical modeling tactics as a powerful means of exploring the inherent synergistic nature of solvation interactions at charged electrochemical interfaces. Further studies along these lines are ongoing in our laboratory.

Acknowledgment. This research is supported by the National Science Foundation.

JA952321U

(27) Stuve, E. M.; Kizhakevariam, N. *J. Vac. Sci. Technol.* **1993**, *A11*, 2217.

(28) Kizhakevariam, N.; Stuve, E. M.; Döhl-Oelze, R. *J. Chem. Phys.* **1991**, *94*, 670.

(29) See, for example: Nørskov, J. K. In *The Chemical Physics of Solid Surfaces*; King, D. A., Woodruff, D. P., Ed.; Elsevier: Amsterdam, 1993; Vol. 6, Chapter 6.

(30) See, for example: Chandrasekhar, J.; Jorgensen, W. L. *J. Chem. Phys.* **1982**, *77*, 5080.

(31) Obtained from the kinetic analysis in ref 32, assuming a preexponential factor of 10^{13} s^{-1}.

(32) Redhead, P. A. *Vacuum* **1962**, *12*, 203.

(33) Maschoff, B. L.; Cowin, J. P. *J. Chem. Phys.* **1994**, *101*, 8138.

(34) *CRC Handbook of Chemistry and Physics*, 67th ed.; CRC Press: Boca Raton, FL, 1986−7; pp E58−E60.

(35) (a) Baetzold, R. C. *J. Phys. Chem.* **1983**, *87*, 3858. (b) Shustorovich, E. *J. Phys. Chem.* **1982**, *86*, 3114. (c) Shustorovich, E. Baetzold, R. C. *Appl. Surf. Sci.* **1982**, *11/12*, 693.